Materials Chemistry | Hot Paper |

Magnetic Phase Transitions in a Ni_4O_4-Cubane-Based Metal–Organic Framework

Muhammad Arif Nadeem,[a] Maggie Chai Cin Ng,[b] Jan van Leusen,[c] Paul Kögerler,*[c, d] and John Arron Stride*[b]

Abstract: An unprecedented spin cluster-based network architecture {[Ni^{II}_2(pdaa)$(OH)_2(H_2O)$]$_n$ (H_2pdaa = 1,4-phenylene diacetic acid)}, comprising 1D linear chains of Ni^{II} ions cross-linked via Ni_4O_4 cubanes, forms under hydrothermal conditions; this 3D coordination network exhibits magnetic ordering at 23.9 K as well as a second magnetic ordering process at 2.8 K likely associated with a structural phase transition.

Introduction

Interest in molecule-based magnetic materials has greatly increased over the last decade, primarily driven by the fact that such materials can help the understanding of magneto-structural correlations and the fundamental phenomena of magnetism at the intersection of molecular to extended magnetic systems; some may even lead to applications.[1] In addition to the nature of the metal spin centers, the bulk magnetic properties mainly depend on the bridging modes and geometries of the bridging ligands. Since the structural factors governing the exchange coupling between paramagnetic centers are complex and in part remain elusive, the pursuit of designed polynuclear complexes and extended networks with predictable magnetic properties continues to be challenging. Magnetic phenomena such as ferromagnetic, ferrimagnetic, and antiferromagnetic long-range ordering at low temperatures have been observed for many transition metal coordination compounds.[2] In contrast, only relatively few magnetically ordered complexes exhibit magnetic phase transitions (MPTs) such as metamagnetic phase transitions. In most cases of porous extended systems displaying bulk ordering phenomena, MPTs are associated with solvation/desolvation.[3] In order to gain bulk magnetic ordering, a strategy to connect various building blocks, that is, single-molecule magnets (SMMs) or single-chain magnets (SCMs), covalently or through cooperative van der Waals forces to fabricate 3D network materials, has recently been adopted.[4] Meanwhile, materials showing multiple MPTs remain scarce. Cheng et al. reported a 3D nickel-organic framework that exhibits canted antiferromagnetism at 5.0 K whilst below this temperature slow relaxation was also observed.[5] Recently, Elizabeth et al. studied an order-disorder phase transition in the cobalt-based MOF $(CH_3)_2NH_2Co(CHOO)_3$.[6] This material displayed antiferromagnetic ordering below 15 K and a second magnetic transition at ca. 11 K. We herein report the first example of a $Ni^{II}_4O_4$ cubane-based 3D network, isolated as [Ni^{II}_2(pdaa)$(OH)_2(H_2O)$]$_n$ (**1**), that exhibits multiple magnetic phase transitions, specifically at 23.9 K and 2.8 K.

Compound **1** was hydrothermally synthesized and crystallizes in the tetragonal space group $I4_1/a$ ($Z = 16$). Analysis of the single-crystal X-ray diffraction data indicates two main structural features: (a) Linear chains of Ni^{II} atoms running perpendicular to each other (along *a* and *b*, Figure 1 a) that are assembled and interlinked by pdaa ligands (Figure 1 b). Each chain consists of two alternating types of Ni^{II}_{chain} centers (Ni1 and Ni2) in the same NiO_6 coordination environment, but with slightly different bond distances and angles, and separated by 3.057 Å. Each Ni^{II} chain site is coordinated by four O atoms belonging to four different pdaa ligands and two O atoms of two different OH^- (O6W) ions (Ni-O: 1.977(2)–2.172(3) Å, O-Ni-O: 80.20(10)–179.999(1)°), resulting in a slightly distorted octahedral geometry. (b) Distorted Ni_4O_4 cubane units bridging the chains (Figure 1 c). Each S_4-symmetric Ni_4O_4 cubane moiety consists of one type of nickel center (Ni3), which is connected with three different oxygen atoms (μ_3-O) of bridging OH^-

[a] Prof. M. A. Nadeem
Department of Chemistry, Quaid-i-Azam University
Islamabad 45320 (Pakistan)
[b] Dr. M. C. C. Ng, Prof. J. A. Stride
School of Chemistry, University of New South Wales
Sydney, NSW 2052 (Australia)
E-mail: j.stride@unsw.edu.au
[c] Dr. J. van Leusen, Prof. Dr. P. Kögerler
Institute of Inorganic Chemistry, RWTH Aachen University
Landoltweg 1, 52074 Aachen (Germany)
E-mail: paul.koegerler@ac.rwth-aachen.de
[d] Prof. Dr. P. Kögerler
Jülich-Aachen Research Alliance (JARA-FIT) and
Peter Grünberg Institute (PGI-6)
Forschungszentrum Jülich, 52425 Jülich (Germany)
Supporting information and the ORCID identification number(s) for the author(s) of this article can be found under: https://doi.org/10.1002/chem.202000867.

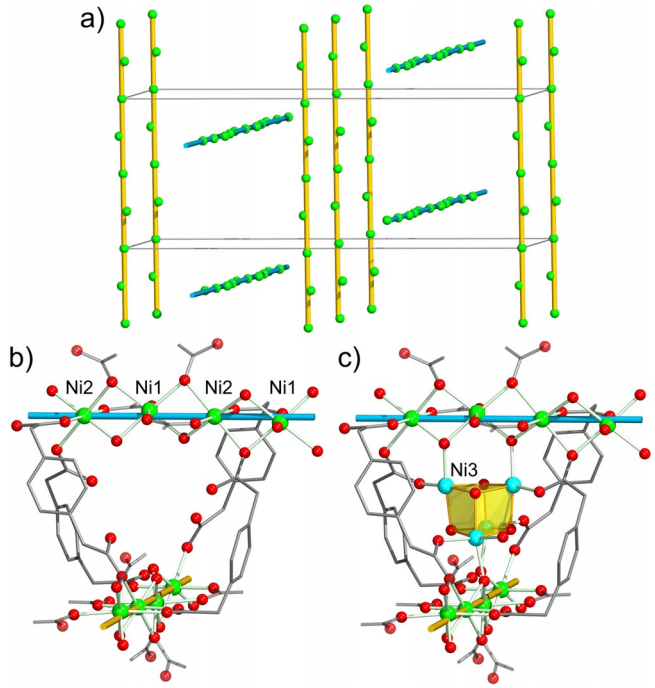

Figure 1. a) Simplified representation of the Ni chains running along *a* (light-blue rods) and along *b* (orange rods) in the crystal lattice of **1**, with the outlines of one unit cell (gray lines). b) A segment of **1** highlighting the connections between neighboring perpendicular Ni chains. c) The same fragment including the Ni_4O_4 cubane unit. Ni_{chain}: green, Ni_{cube}: light blue, O: red spheres, C: gray sticks; some pdaa units shown as incomplete fragments. Coordinative (Ni-O) bonds: pale green (chains) or orange (cube). H omitted for clarity.

groups of the Ni_4O_4 cubane unit, one oxygen atom (O6W) that links the Ni3 atom to the linear chains, one oxygen atom (O7) of a pdaa ligand and one water molecule (O4), to yield a distorted octahedral geometry (Ni3-O: 2.003(2)–2.125(3) Å, O-Ni3-O: 81.84(11)–179.999(1)°). The asymmetrical structural, coordination environment of all three nickel centers and Ni_4O_4 cubane cluster are shown in Figures S4 and S5 of supporting information. The uniform +II oxidation state of all three nickel sites are confirmed by bond valence sum analysis ($\Sigma_{bv}(Ni^{II})$ = 1.993–2.168).

In the Ni_4O_4 cubane, four Ni···Ni distances are equal to 3.069 Å, with the remaining two Ni···Ni distances of 3.072 Å, both below the mean literature value of 3.11 Å calculated by Isele et al.[7] The six faces of the cubane are not all equivalent, with the four side faces (parallel to the *c* axis) having Ni-O-Ni bridging angles in the range of 96.92°–97.74°, whereas the top and bottom faces (perpendicular to the *c* axis) have Ni-O-Ni angles of 97.34°. Each Ni3 atom is linked to Ni1 and Ni2 centers of the 1D linear chains via OH^- groups above and below the Ni_4O_4 cubane at a distance of 3.644 Å and 3.407 Å, respectively. The single, crystallographically unique pdaa separates the two linear chains via two different carboxylate groups at a distance of 8.776 Å. Two oxygen atoms (O1 and O2) of one carboxylate coordinates with the two different Ni atoms (Ni1 and Ni2) in a *syn–syn* $\eta^1{:}\eta^1{:}\mu_2$ chelating mode, whilst one oxygen atom (O7) of the second carboxylate group coordinates a Ni^{II}_{cubane} center and a second oxygen atom (O5) bridges the two Ni^{II} centers of neighboring linear chains. The two flexible arms of the pdaa ligand are directed towards the same side and twist perpendicular to each other to coordinate to the Ni_{chain} centers, bridged via Ni_4O_4 cubanes, to form a 3D network (Figure 2).

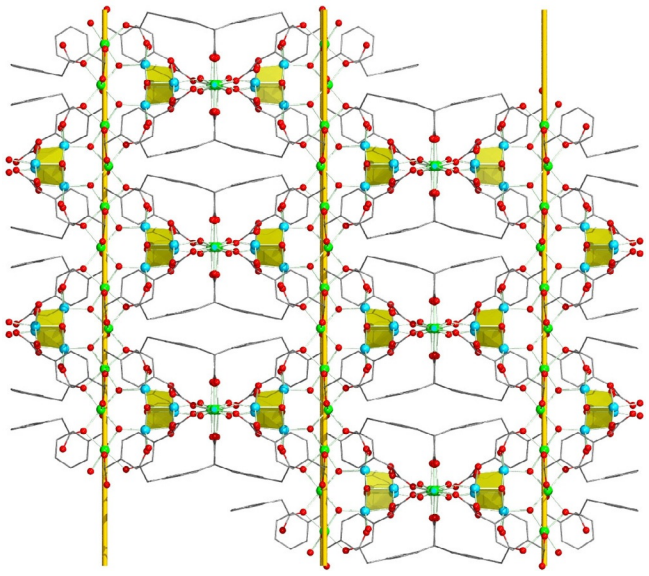

Figure 2. A packing diagram of **1** indicating how the 1D Ni chains are separated via Ni_4O_4 cubane units. Color code as in Figure 1. H omitted for clarity.

Results and Discussion

Magnetochemical properties

Magnetic measurements of compound **1** in static magnetic fields are summarized in Figure 3. At 300 K and 0.1 T, $\chi_m T$ = 2.68 $cm^3\,K\,mol^{-1}$ lies within the expected range of 1.96–3.06 $cm^3\,K\,mol^{-1}$ for two non-interacting Ni^{II} centers.[8] With decreasing temperature, $\chi_m T$ slightly increases until ca. 50 K, subsequently showing a sharp and very pronounced maximum at ca. 20 K and then dropping down to a minimum at 3.5 K, only to rise once again to 3.52 $cm^3\,K\,mol^{-1}$ at 2.0 K. The corresponding inverse molar magnetic susceptibility (Figure 3a, inset) is characterized by a linear behavior for most of the temperatures ($T > 20$ K), a plateau in the range from 20 to 4.5 K, and another decreasing curve below 4.5 K down to 2.0 K. Besides FC (field cooling) measurements, we additionally measured the sample at ZFC (zero field cooling), but found only marginal differences between both measurements for data below 20 K (as indicated by the marginal displacement of the data at these temperatures in Figure 3a).

While the first maximum can be unambiguously assigned to predominant ferromagnetic exchange interactions between the Ni^{II} centers of **1**, the subsequent occurrence of the minimum combined with the increase of $\chi_m T$ for the lowest temperatures could be due to impurities. We, thus, measured multiple, individually synthesized batches of **1** to find that all yielded virtually identical data. Therefore, we can, with near certain-

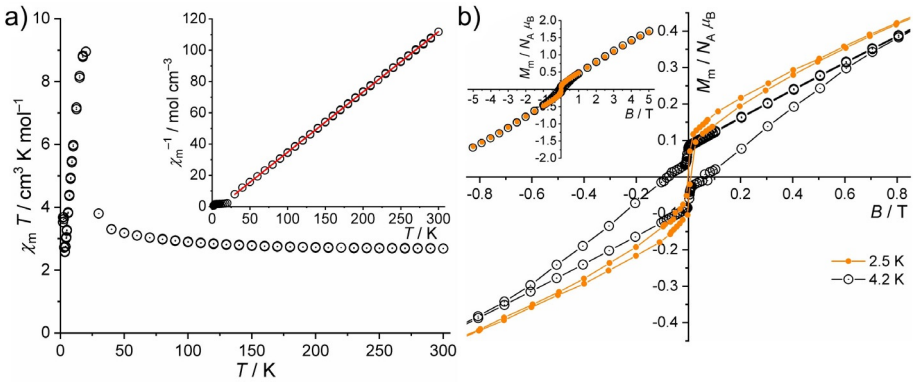

Figure 3. a) Temperature dependence of $\chi_m T$ at 0.1 T of **1**, ZFC and FC measurements, and inverse molar magnetic susceptibility χ_m^{-1} vs. temperature T (inset). b) Molar magnetization M_m vs. applied field B at 2.5 and 4.2 K over the range $-0.8 \leq B \leq +0.8$ T, and over the entire field range (± 5.0 T; inset); connecting lines are shown as a guide to the eye. Experimental data shown as circles, the least-squares fit to Curie–Weiss expression as red solid line.

ty, exclude impurity levels as significantly affecting the magnetic properties of **1** at low temperatures. Since octahedral Ni^{II} centers can be approximately interpreted as effective isotropic spin centers with $S_{eff} = 1$, we analyzed the linear segment of the χ_m^{-1} vs. T curve in terms of the Curie–Weiss law $\chi_m = C / (T - \theta_W)$. The least-squares fit yields $C = (2.595 \pm 0.003)$ cm^3 K mol^{-1} and $\theta_W = (9.76 \pm 0.20)$ K. The Weiss temperature confirms the predominant ferromagnetic exchange interactions (since $\theta_W > 0$). In addition, we derive the (mean) effective g factor from the Curie constant as $g_{eff} = (2.28 \pm 0.01)$ for each Ni^{II} center, fully in line with the expected value for an octahedrally coordinated Ni^{II} ion.

The molar magnetization M_m was studied as function of the applied external magnetic field B at 2.5 K and 4.2 K, that is, at temperatures above and below the minimum of the $\chi_m T$ vs. T curve, which are still small enough to result in sufficiently large magnetization values in order to detect hysteretic behavior. Both magnetization curves are similar for fields with magnitudes larger than ca. 1 T, for which they almost linearly increase up to 1.7 N_A μ_B at 5.0 T. However, they significantly differ at fields between ± 0.8 T: At 2.5 K, the magnetization gradually approaches a value of ca. ± 0.1 N_A μ_B for decreasing magnitudes of the magnetic field, yet the magnetization rapidly vanishes at the lowest fields showing a marginal or zero remanent magnetization. On the other hand, at 4.2 K, we find an open hysteresis loop with a remanent magnetization of 0.07–0.08 N_A μ_B, a coercivity of 0.07–0.08 T, and magnetization steps at ca. ± 0.02 T (and maybe another pair of steps at ca. ± 0.06 T).

Since the magnetization does not reach saturation at 5.0 T, and since the M_m value of 1.7 N_A μ_B is well below the estimated saturation value of 4.6 N_A μ_B (i.e. 2.3 N_A μ_B per Ni^{II} center, derived from $M_{m,sat} = g_{eff}$ S_{eff} N_A μ_B), the ground state of **1** cannot be characterized by fully collinear ferromagnetic exchange interactions. Thus, either a minor amount of exchange pathways with antiferromagnetic interactions is present within the compound, or chains or areas of opposing magnetic moments exist in the rather complicated structure (or some combination of both). Considering that magnetization values for paramagnetic compounds decrease with increasing temperatures at a constant applied field, M_m at 5.0 T should be larger at 2.5 K than at 4.2 K. This is not observed. In addition, since the behavior of the magnetization drastically changes, the magnetization rather indicates a structural phase transition between 2.5 K and 4.2 K. Besides the observation of hysteresis at 4.2 K, the magnetization steps point to the presence of a (thermally assisted) resonant tunneling mechanism as known for example, for quasi-zero dimensional spin systems such as SMMs.[9] One prerequisite for the presence of such a mechanism is a magnetically anisotropic system, which can be assumed for **1** given its structure. However, **1** represents an extended infinite spin system; a porous metal organic framework composed of chains and knots of Ni^{II} centers, at the same time, the complex magnetic exchange topology of **1** does also not constitute a classical three-dimensional bulk ferromagnet.

To gain further insight into the magnetism of **1**, we also probed dynamic magnetic fields of various frequencies in the absence of a static bias field. The corresponding ac susceptibility data are shown in Figure 4–Figure 6. As evident from the temperature dependence of the out-of-phase molar magnetic susceptibility χ_m'' (Figure 4), there are two temperature ranges in which χ_m'' significantly differs from zero: between 17 and 25 K and between 2.0 and 3.0 K. In the higher temperature range, shown in detail in the insets of Figure 4, the out-of-phase signal is small, but shows a temperature dependence that is similar to a phase transition to long range ordering in a 3D ferromagnet,[10] yet the order of magnitude is much smaller for **1**. On the other hand, compounds composed of a few interacting paramagnetic centers—except for SMMs—do not show such a characteristic feature. According to structural information, **1** is a three dimensional, rather asymmetrical mesh with large vacancies that could allow for a partial ordering along for example, the Ni^{II} chains and/or knots, analogous to the long-range ordering in a ferromagnet. From the inflection point of χ_m'' vs. T, the corresponding ordering temperature amounts to $T_o = (23.9 \pm 0.2)$ K.

Relevant out-of-phase signals at the lowest temperatures span a very small range of less than 1 K between 2.0 and 3.0 K; the signals vanish below 2.0 K and above 2.8 K. The maximum values of χ_m'' are much larger compared to the ones observed

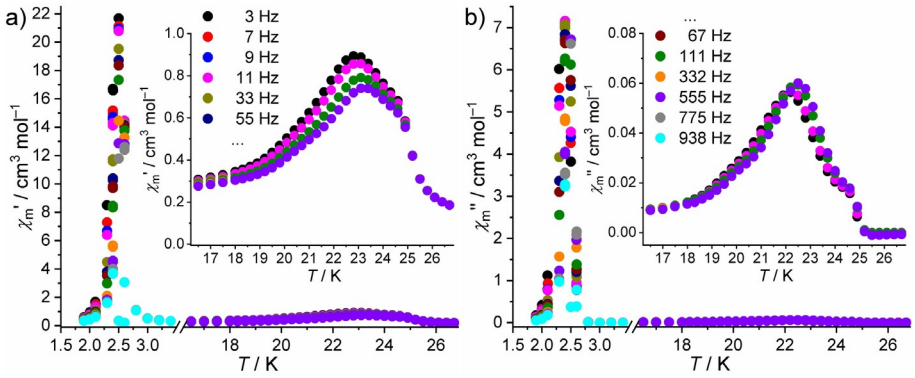

Figure 4. a) Temperature dependence of ac in-phase molar susceptibility χ_m' at zero bias field and various frequencies of **1**, and in detail for $16 \leq T \leq 27$ K (inset). b) AC out-of-phase molar susceptibility χ_m'' vs. temperature *T*, and in detail for $16 \leq T \leq 27$ K (inset); experimental data (full circles).

at 17 to 25 K. Since the χ_m'' vs. *f* curves at 2.4 K and 2.5 K reveal maxima (Figure 5), as also evident from the Cole–Cole plot (χ_m'' vs. χ_m', Figure 6), we analyzed the data in terms of a generalized Debye expression.[11] However, none of the fits could reasonably reproduce the data. Introducing several types of restrictions also failed to model the data using the extended Debye expression, which leads to the conclusion that the ratio of the (average) conserved energy to the dissipated energy per cycle depends on the applied frequency of the magnetic field. Thus, relaxation processes solely caused by magnetic ordering are highly unlikely. Considering the very steep and narrow maxima observed in the χ_m' vs. *T* and χ_m'' vs. *T* curves that occur within a very small temperature interval (ca. 2.1–2.6 K, Figure 4), the relaxation processes are potentially rather fast compared to the characteristic timescales of SMMs.

Combining the analyses of ac and dc magnetic data of **1**, leads us to conclude a partial magnetic ordering for $T \leq 23.9$ K, and another magnetic ordering process at about 2.8 K, which presumably additionally involves a structural phase transition.

The identified magnetic properties can be qualitatively rationalized from the structural properties of **1**. The chains and the Ni_4O_4 cubanes consist of close neighboring Ni^{II} centers with Ni···Ni distances less than 3.1 Å and Ni-O-Ni angles ranging from 90.8° to 99.8°, that is, between 90° and 100°. While the distance is correlated to the magnitude of the exchange interactions (the closer, the larger), the angles determine the type of interaction considering the well-known Kramers–Anderson superexchange model.[12] For most Ni-O-Ni angles, the exchange interaction are antiferromagnetic, in particular, for most obtuse angles larger than about 100°. However, for Ni-O-Ni angles close to 90°, the interaction becomes ferromagnetic. Therefore, the Ni^{II} centers forming the chains as well as the cubanes are likely the origin of the predominantly ferromagnetic

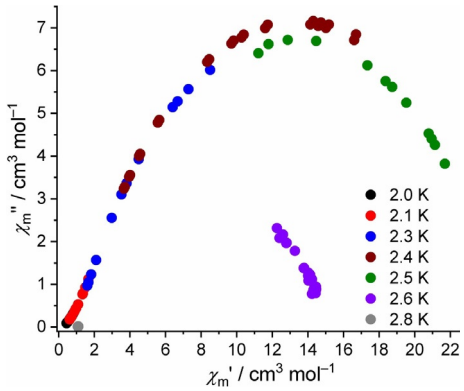

Figure 6. Cole–Cole plot of ac out-of-phase molar susceptibility χ_m'' vs. in-phase molar susceptibility χ_m' at zero bias field between 2.0 and 2.8 K; experimental data (colored full circles).

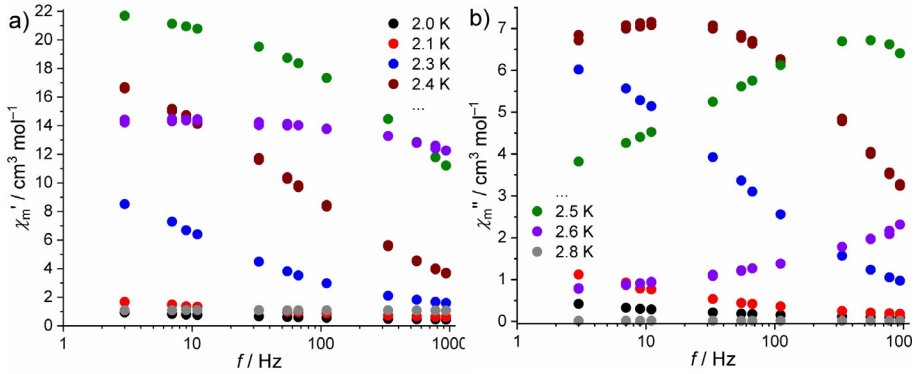

Figure 5. a) Frequency dependence of ac in-phase molar susceptibility χ_m' at zero bias field between 2.0 and 2.8 K. b) Corresponding ac out-of-phase molar susceptibility χ_m''; experimental data (full circles).

interactions of 1. The chains and the cubanes are linked by OH^- groups yielding closest Ni···Ni distance of 3.4 Å and Ni-O-Ni angles of 118°. Thus, the interactions via these exchange pathways are likely to be antiferromagnetic and weaker than the ferromagnetic interactions within the chains and cubanes, providing an explanation for the observed magnetization data.

Conclusions

In conclusion, a 3D MOF based on perpendicular 1D Ni^{II} linear chains interconnected via Ni_4O_4 cubanes has been synthesized, offering a rare example of a magnetic material that shows several partial magnetic ordering phenomena: one at $T \leq 23.9$ K, and another process at about 2.8 K, likely associated with a structural phase transition. These results demonstrate the concept of utilizing MOF architectures to connect extended spin structures with molecular spin clusters in order to realize novel or complex magnetic-ordering phenomena.

Experimental Section

Elemental analyses were performed on a Carlo Erba EA 1108

FTIR spectra (KBr pellets, 400–4000 cm^{-1}) were recorded on a Thermo Nicolet Avatar 320 spectrometer. Magnetic data of **1** were recorded using a Quantum Design MPMS-5XL SQUID magnetometer. The polycrystalline sample was compacted and immobilized into a cylindrical PTFE capsule. DC susceptibility data were acquired as a function of the magnetic field (−5.0 to +5.0 T at 4.2 K) and temperature (2.0–300 K at 0.1 T); ac data were measured in the absence of a static bias field in the frequency range 1–1000 Hz (T = 1.9–50 K, B_{ac} = 3 G). Data were corrected for the diamagnetic contributions of the sample holder and the compound ($\chi_{dia} = -1.78\times10^{-4}$ $cm^3\,mol^{-1}$).

Powder X-ray diffraction data were recorded on a Philips X'Pert diffractometer ($Cu_{k\alpha}$, λ = 1.54056 Å) to check the purity of bulk samples of **1** (Figure S1 in the Supporting Information). Thermogravimetric analyses were performed under nitrogen flux using a Mettler Toledo TGA/SDTA 851 at a heating rate of 10 °C min^{-1} to assess the thermal stability of **1** (Figure S2 in the Supporting Information). **1** is thermally stable up to 380 °C. An initial weight loss (ca. 5%) starting at 150 °C is due to loss of one water molecule coordinated to Ni3 (calc. 5.06%) in the framework. At higher temperatures the mass remains constant, followed by sudden decrease in the weight, suggesting the onset of decomposition around 380 °C with a total weight loss of 55.3% (calc. 57.98%), resulting in simple oxides (NiO). Suitable single crystals of **1** ($0.13\times0.10\times0.05$ mm^3) were used in the intensity data collection using a Bruker SMART APEX CCD diffractometer at 150(2) K (λ = 0.71073 Å). The structures were solved by direct methods and refined by full-matrix least squares against F^2 using the SHELXS-97 and SHELXL-97 programs.[13] Anisotropic thermal parameters were assigned to all non-hydrogen atoms. The hydrogen atoms were set in calculated positions and refined as riding atoms with a common fixed isotropic thermal parameter. Analytical expressions of neutral atom scattering factors were employed, and anomalous dispersion corrections were incorporated.

Synthesis of 1

A mixture of 0.5 mmol of 1,4-phenylene diacetic acid (0.097 g) and 2 mmol of KOH (0.112 g) in 6 mL distilled water was stirred for 10 minutes followed by addition of a solution of $NiCl_2{\cdot}6H_2O$ (1 mmol, 0.237 g) in 4 mL H_2O. The resulting solution was sealed in a 23 mL Teflon-lined stainless steel autoclave and heated to 170 °C for three days under autogenous pressure. The reaction vessel was then cooled to room temperature over 4 hours. Green diamond-shaped crystals of **1** suitable for single-crystal X-ray diffraction analysis were collected from the final reaction system by filtration and dried in air at ambient temperature (42% yield based on Ni). Anal. calcd: C, 33.7% H, 1.7%. Found: C, 33.4% H, 3.31%. IR data (ν_{max}/cm^{-1}): 3672 s, 3591 s, 3569 s, 3353 s, 2965w, 2930 m, 1607 s, 1556sd, 1427 s, 1386 s, 1280 m, 1202w, 1138 m, 940 s, 803 s, 737 s (Figure S3).

Crystallographic data for 1

$C_{10}H_6Ni_2O_7$, M_r = 355.57 g mol^{-1}, tetragonal, space group $I4_1/a$, a = 12.1839 (6), b = 12.1839 (6), c = 33.0206 (18) Å, V = 4901.8 (4) $Å^3$, T = 150(2) K, Z = 16, ρ_{calcd} = 1.927 g cm^{-3}, λ = 0.7107 Å, 8548 reflections collected, 1812 unique (R_{int} = 0.037), $R[F^2 > 2\sigma(F^2)] = 0.031$ and $wR(F^2) = 0.086$, S = 1.05.

Acknowledgements

Part of this work has been supported by a Georg Forster fellowship of the Alexander von Humboldt Foundation (M.A.N.).

Conflict of interest

The authors declare no conflict of interest.

Keywords: cubanes · magnetic materials · metal–organic frameworks · nickel · phase transitions

[1] a) O. Kahn, *Acc. Chem. Res.* **2000**, *33*, 647; b) M. Gibertini, M. Koperski, A. F. Morpurgo, K. S. Novoselov, *Nat. Nanotechnol.* **2019**, *14*, 408; c) M. Sakamoto, K. Manseki, H. Ökawa, *Coord. Chem. Rev.* **2001**, *379*, 219; d) C. Benelli, D. Gatteschi, *Chem. Rev.* **2002**, *102*, 2369; e) I. Ciofini, C. A. Daul, *Coord. Chem. Rev.* **2003**, *187*, 238; f) A. Lakma, S. M. Hossain, J. van Leusen, P. Kögerler, A. K. Singh, *Dalton Trans.* **2019**, *48*, 7766.

[2] a) E. Coronado, F. Palacio, J. Veciana, *Angew. Chem. Int. Ed.* **2003**, *42*, 2570; *Angew. Chem.* **2003**, *115*, 2674; b) Z. Fu, Y. Zheng, Y. Xiao, S. Bedanta, A. Senyshyn, G. G. Simeoni, Y. Su, U. Rücker, P. Kögerler, T. Brückel, *Phys. Rev. B* **2013**, *87*, 214406; c) C. Janiak, *Dalton Trans.* **2003**, 2781; d) P. Day, A. E. Underhill, *Philos. Trans. R. Soc. London Ser. A* **1999**, *357*, 3163 – 3184.

[3] a) X. Zhang, M. R. Saber, A. P. Prosvirin, J. H. Reibenspies, L. Sun, M. B. Rivas, H. Zhao, K. R. Dunbar, *Inorg. Chem. Front.* **2015**, *2*, 904; b) W. Kaneko, M. Ohba, S. Kitagawa, *J. Am. Chem. Soc.* **2007**, *129*, 13706; c) J. A. R. Navarro, E. Barea, A. Rodríguez-Diéguez, J. M. Salas, C. O. Ania, J. B. Parra, N. Masciocchi, S. Galli, A. Sironi, *J. Am. Chem. Soc.* **2008**, *130*, 3978; d) D. Maspoch, D. Ruiz-Molina, K. Wurst, N. Domingo, M. Cavallini, F. Biscarini, J. Tejada, C. Rovira, J. Veciana, *Nat. Mater.* **2003**, *2*, 190.

[4] a) J. Yoo, W. Wernsdorfer, E.-C. Yang, M. Nakano, A. L. Rheingold, D. N. Hendrickson, *Inorg. Chem.* **2005**, *44*, 3377; b) H. Miyasaka, K. Nakata, L. Lecren, C. Coulon, Y. Nakazawa, T. Fujisaki, K. Sugiura, M. Yamashita, R. Clérac, *J. Am. Chem. Soc.* **2006**, *128*, 3770; c) H. Miyasaka, K. Nakata, K. Sugiura, M. Yamashita, R. Clérac, *Angew. Chem. Int. Ed.* **2004**, *43*, 707; *Angew. Chem.* **2004**, *116*, 725; d) O. Roubeau, R. Clérac, *Eur. J. Inorg. Chem.* **2008**, 4325; e) H. Miyasaka, K. Takayama, A. Saitoh, S. Furukawa, M. Yamashita, R. Clérac, *Chem. Eur. J.* **2010**, *16*, 3656.

[5] F.-P. Huang, J.-L. Tian, D.-D. Li, G.-J. Chen, W. Gu, S.-P. Yan, X. Liu, D.-Z. Liao, P. Cheng, *Inorg. Chem.* **2010**, *49*, 2525.
[6] R. Yadav, D. Swain, H. L. Bhat, S. Elizabeth, *J. Appl. Phys.* **2016**, *119*, 064103.
[7] K. Isele, F. Gigon, A. F. Williams, G. Bernardinelli, P. Franz, S. Decurtins, *Dalton Trans.* **2007**, 332.
[8] H. Lueken, *Magnetochemie*, Teubner, Stuttgart, **1999**.
[9] a) M. A. Novak, R. Sessoli, in *Quantum Tunneling of Magnetization* (Eds.: L. Gunther, B. Barbara), Kluwer, Dordrecht, **1995**, pp. 171 – 188; b) C. Paulsen, J. G. Park, in *Quantum Tunneling of Magnetization* (Eds.: L. Gunther, B. Barbara), Kluwer, Dordrecht, **1995**, pp. 189 – 207; c) J. R. Friedman, M. P. Sarachik, J. Tejada, J. Maciejewski, R. Ziolo, *J. Appl. Phys.* **1996**, *79*, 6031.
[10] M. Bałanda, *Acta Phys. Pol. A* **2013**, *124*, 964.
[11] K. S. Cole, R. H. Cole, *J. Chem. Phys.* **1941**, *9*, 341.
[12] a) H. A. Kramers, *Physica* **1934**, *1*, 182; b) P. W. Anderson, *Phys. Rev.* **1950**, *79*, 350.
[13] G. M. Sheldrick, *SHELXS 97*, Program for the Solution of Crystal Structures; University of Göttingen: Germany, **1997**.

Manuscript received: February 18, 2020
Revised manuscript received: March 25, 2020
Accepted manuscript online: April 3, 2020
Version of record online: May 14, 2020

